Spectroscopic ellipsometry and photovoltaic characteristics for n-CdS/p-Cu_2ZnSnS_4 heterojunction by annealing for solar cells

A. Almohammedi[a,*], E. R. Shaaban[b]
[a]*Department of Physics, Faculty of Science, Islamic University of Madinah, Al Jamiah, Madinah 42351, Saudi Arabia*
[b]*Physics Department, Faculty of Science, Al–Azhar University, Assuit, 71542, Egypt*

Owing to its direct bandgap in the range to be used as an absorbent material and due to its high absorption rate, kesterite Cu_2ZnSnS_4 (CZTS) is a p-type prospective absorber material (with thickness 500 nm) for solar cell applications. Kesterite Cu_2ZnSnS_4 (CZTS) thin films were prepared using the thermal evaporation technique. The (CZTS) thin films were annealed at different annealing temperatures chosen according to TGA analysis in the range of (400°C, 450°C, 475°C, and 500°C). The influence of annealing temperatures on the structural, morphology and optical properties of the CZTS films was investigated. The XRD patterns and Raman spectra have revealed the formation of CZTS thin with a high-quality crystal structure. The optical constants refractive index n, and extinction coefficient, k consequently band gap are estimated from SE via construction an optical model. The refractive index *n* of the CZTS /glass films received from SE model increases with the annealing temperature that is credited to the rise of the size of the crystal. It was also found that when the annealing temperature of the CZTS layer increases, the general behavior of the extinction coefficient k of the CZTS /glass film increases. In addition, it is found that the direct optical transition with energy band gap is compact from 1.75 eV at RT to 1.49 eV at maximum crystallization 500 °C. The Ni/n-CdSe/p-CdTe/Pt heterojunction has been successfully assembled. The dark and illumination (current-voltage) behavior of fabricated heterojunctions had been suggested at distinctive different annealing of CZTS layer, as well as for voltages ranging from -2 to 2 volts.

(Received June 15, 2022; Accepted October 11, 2022)

Keywords: Cu_2ZnSnS_4, Thin films, Spectroscopic ellipsometry, Optical bandgap, Ni/n-CdSe/p-CdTe/Pt heterojunction, Electric properties

1. Introduction

Developing and finding new Sustainable energy sources are very vital and have got great attention. Solar energy is promising because it is a clear, convenient, and sustainable source. Nowadays many researchers in the field of materials science and nanotechnology aim to increase the efficiency of solar cells. The main challenge in photovoltaics technology is to achieve high efficiency, low cost, and inclusion of abundant natural materials [1].

Cadmium Telluride (CdTe) and Copper Indium Gallium Selenide (CIGS) are used to be important materials for commercial thin-film photovoltaic devices, because of their moderate efficiencies, but they are toxic and expensive [2, 3].

Cu_2ZnSnS_4 (CZTS) compound has received great interest during the late decade as an absorber for solar cell device applications. Kesterite CZTS is a p-type semiconductor with a bandgap energy of 1.5 eV, a high absorption coefficient (>104 cm^{-1}) in the visible range spectrum, and containing only earth-abundant low toxicity elements [4 -7].

Since the quality of the CZTS film surface has a crucial role in the solar cell operation, many physical and chemical methods have been used to grow Cu_2ZnSnS_4 thin films such as spin coating [8], sputtering [9-11], thermal evaporation [12, 13], Pulsed Laser Deposition (PLD) [14, 15], the sulfurization of electron-beam-evaporated precursors [16] and spray pyrolysis [17–19].

* Corresponding author: arda@iu.edu.sa
https://doi.org/10.15251/CL.2022.1910.701

Until far, the greatest documented power conversion efficiency (*PCE*) for pure sulfide compounds in the corresponding form: CZTS equals 9.2% according to the related work [20]. On the other side, this quantity was for pure selenide $Cu_2ZnSnSe4$ with chemical abbreviated form: (CZTSe) is 11.6% [21]. Furthermore, the power conversion efficiency of the mixed sulfide-selenide compound is 12.6% [22]. Nevertheless, CZTS solar cells have a lower *PCE* than CIGS or CdTe (21.7%) [23].

In this work, CZTS thin films were prepared using the thermal evaporation technique on the pre-cleaned glass substrates to study its structural and optical properties at different temperatures (400^{o}C, 450^{o}C, 475^{o}C, and 500^{o}C) according to the thermal analysis of TGA and DSC. The annealing temperature was below 550^{o}C to avoid Sulfur escape and the decomposition of CZTS thin films to different binary phases such as $Cu_{2-x}S$, ZnS, and SnS [24]. The effect of annealing temperature on the structural, morphological, optical, and electrical characterization of CZTS thin films was investigated. For the first time spectroscopic ellipsometry were used as the best method to estimate the optical parameters thus the energy gap of investigated annealed CZTS films. The Ni/n-CdSe/p-CdTe/Pt heterojunction has been successfully assembled. The dark and illumination (current-voltage) traits of fabricated heterojunctions had been suggested at distinctive different annealing of CZTS layer, as well as for voltages ranging from -2 to 2 volts.

2. Experimental procedures

2.1. Materials

Copper (II) nitrate $Cu(NO_3)_2$, Zinc acetate $Zn(CH_3COO)_2$, Stannous chloride ($SnCl_2$) , Citric acid ($C_6H_8O_7$), deionized water, sulfide amine solution, distilled water and pure alcohol were used for CZTS thin film fabrication. All the used chemicals and precursors were utilized without any further purification.

2.2. Preparation of CZTS thin film

For the fabrication of CZTS nanoparticles, aqueous solution containing $Cu(NO_3)_2$, $Zn(CH_3COO)_2$ and $SnCl_2$ precursors that were dissolved with mixture 2, 1, and 1 mol/L was prepared. Citric acid ($C_6H_8O_7$) and deionized water were added with molar ratio 1:3 of metal ions to citric acid. A transparent solution was obtained with stirring the aqueous solution in a flask for about 10 *min*. Citric acid ($C_6H_8O_7$) was utilized as a complexing agent. 4 mL from Sulfide amine solution was added to the flask at temperature 200°C and kept to react for about 30 *min*. Then a centrifuge was utilized to separate the CZTS nanoparticles. To obtain the powder nanoparticles, the final solution was kept to dry in a low temperature vacuum oven. This powder was the starting material to prepare the CZTS films.

To prepare the CZTS film, first the substrates were ultrasonically pre-cleaned by sequential rinses with distilled water and pure alcohol for 15 *min* each then kept drying in air. Thermal evaporation technique was used to prepare the CZTS thin films using (Denton Vacuum DV 502 A) coating unit under high vacuum pressure (10^{-7} mbr) with deposition rate was 20 Å/sec. The substrate temperature was kept 100^{o}C. The thickness of thin films was adjusted using FTM6 thickness monitor by putting the same weight on the boat to get a higher thickness to avoid the effect of film thickness. The film thickness was determined with high precision in terms spectroscopic ellipsometry model.

2.3. Characterization of CZTS thin films

The XRD Philips diffractometry (1710), with Cu-Kα1 radiation (λ = 1.54056 Å) technique was used for structure and the crystalline phase characterization for the thin film samples. A scanning electron microscope (SEM, JOEL XL) of operating voltage of 30 kV, used for surface morphology studies. The optical properties were studied by the spectroscopic ellipsometry (SE) technique. Data collection using spectroscopic ellipsometry was conducted using a SE (VASE, J. A. Woollam Co., Inc). Typically, in SE measurements, two parameters Ψ and Δ were recorded as a function of wavelength. The data were collected at the incident angle of

70^{o} for a spectral range between 300 nm to 1100 nm. The SE data were analyzed by the J. A. Woollam Complete Ease software package. The thermogravimetric analysis of the deposited CZTS film was analyzed utilized a TGA and DSC instrument (Shimadzu 50, accuracy ±0.1 K).

2.4. Photovoltaic measurements

Ni (front electrode)/n-CdS/p-CZTS /Pt (back electrode) heterojunctions were fabricated utilizing deposition of the CdS thin layer on the CZTS layer (~500 *nm*) which was deposited on pre-cleaned glass substrates (5 μm). The front electrode contact was made by depositing a semi-transparent grid of platinum (Pt) fingers (100 *nm*) directly onto the surface of the CZTS layer, while the back contact electrode (nickel, Ni with thickness of 100 *nm*) was contacted with the CdS thin layer deposited directly on the CZTS layer.

The front and back electrode contacts were considered ohmic for the small voltages. The current-voltage (*I–V*) measurements for the generated device were carried out using a standard circuit (Keithley 610 as a voltage source and current meter) to determine the current through the heterojunction. At room temperature, the dark (current-voltage) characteristics were obtained in a completely dark chamber. Under standard experimental conditions, the Keithley 2400 Source Meter device was utilized to measure the illuminated (current -voltage, (*I-V*)) characteristics of the fabricated devices in the solar 1.5 global spectra (AM1.5G) for input power (P_{in}= 184.33 mW/cm^2) generated by Halogen lamp 150W.

3. Results and discussion

To select suitable annealing temperatures for the CZTS nanoparticle, thermogravimetric analysis (TGA) analysis was investigated in published paper of Almohammedi et. Al (2020) [25]. More detail about TGA and its derivative are displayed in ref. [25] The crystallization peak is at 500^{o}C, so the annealing temperatures were chosen from 400-500^{o}C.

Fig. 1 shows the XRD patterns of the as deposited and annealed CZTS thin films at different annealed temperatures. The XRD data have confirmed the formation of crystalline CZTS. All the CZTS thin films show diffraction peaks at 2θ = 28.53°, 47.32° and 56.19°, which are consistent with the diffraction planes of CZTS (112), (220) and (312) (JCPDS-26-0575), respectively, which strongly emphasizes the structure formation of CZTS, which belong to tetragonal phase. Annealed CZTS thin films show sharper (112) peak which indicates better crystal quality with increasing annealing temperature. One can see in Fig. 1 the full width at half maximum (FWHM) values were decreased with increasing annealing temperature, while the size increased as a result of improving the crystallinity.

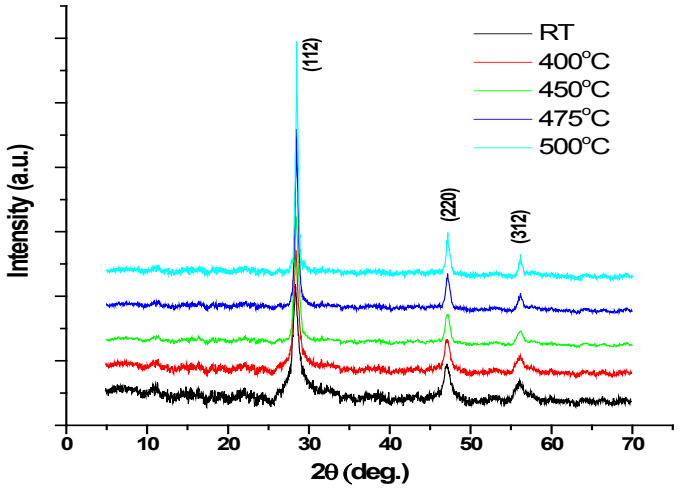

Fig. 1. XRD patterns of unannealed and annealed CZTS thin films at different annealing temperature.

The crystallinity and phase content of the CZTS thin films were further analyzed through Raman spectroscopy. Fig. 2 shows Raman spectra of as-deposited and annealed CZTS thin film samples which were recorded in the spectral range of 100–600 cm^{-1}. It can be shown that the Raman spectra of all the samples are similar. Three Raman modes corresponding to CZTS Kesterite were observed, main peaks at 337 cm^{-1} and weak peaks at 284 cm^{-1}, which indicate the formation of crystalline CZTS thin films with high purity [26, 27]. The main peak at 337 cm^{-1} is shifted to lower energies as the annealing temperature increase, which can be attributed to the existence of internal stress in CZTS films. This phenomenon is known for the annealed CZTS thin films [28]. However, Raman spectroscopy data showed weak peaks at 475 cm^{-1} which are attributed to the Cu_2S phase.

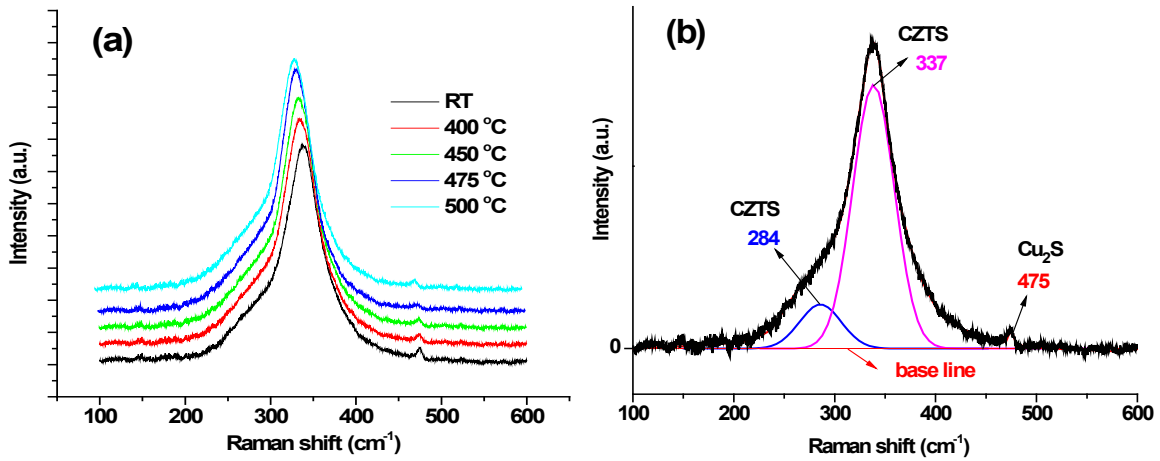

Fig. 2. (a, b). Raman spectra of unannealed and annealed CZTS thin films (a) and deconvolution of CZTS thin films at RT temperature.

Scanning electron micrographs (SEM) were used to study the surface topography of the CZTS thin films and the morphological state development of the growing CZTS thin films with annealing temperature. Fig. 3 displays the SEM images of as-deposited and annealed CZTS thin films at T_a = 500°C. The as-deposited CZTS thin film shows the rough and non-uniform surface distribution. In the structural form of SEM images, some voids can be observed. The surface morphology of the CZTS film has been significantly influenced by annealing. The uniformity of the CZTS films is highly improved, films have become compact and have densely and distinct packed grains' structures. The annealed film appears smoother than the as-deposited thin film. Moreover, fewer voids are present after the annealing process. The grain and its boundaries are more clearly visible with increasing the annealing temperature.

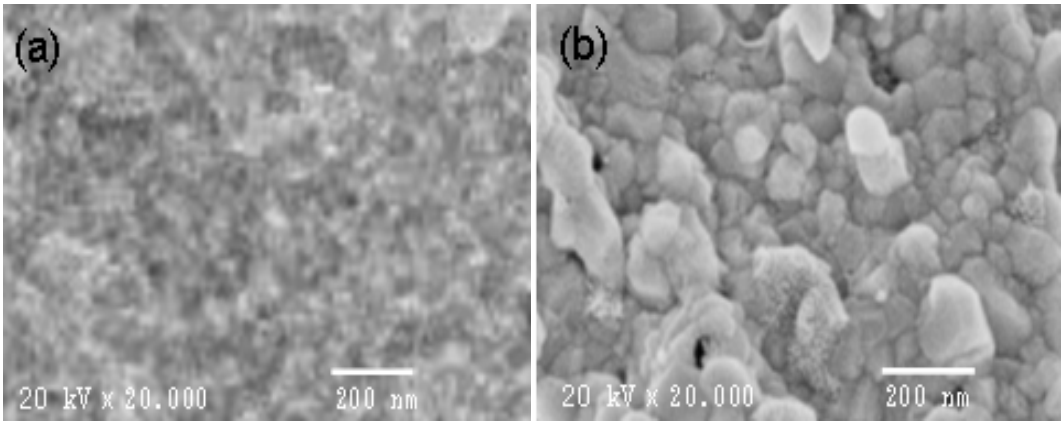

Fig. 3. SEM images of CZTS thin films at temperatures (a) As -deposited and (c) 500 °C.

3.1. Optical properties in terms of Spectroscopic Ellipsometric

The spectroscopic ellipsometric outcomes of CZTS thin films prepared on transparent glass measured by way of SE method changed into within the spectral variety of 300-1100 nm at an prevalence angle of 65°, the information is amassed in intervals of 5 nm. Spectroscopic ellipsometry without delay information angles Ψ,and Δ, which can be connected to the complex mirrored or reflected image coefficients (Fresenal's coefficient) of the polarized light by the subsequent equation [29-31]

$$\rho = \frac{r_p}{r_s} = \tan\psi \exp(i\,\Delta) \tag{1}$$

wherein Ψ, Δ, r_p and r_s are mentioned the angle received from the amplitude ratio among the parallel polarized wave (p) and perpendicularly polarized wave (s), the polarized waves exchange. The Spectral ellipsometric facts ψ_{exp} & Δ_{exp} of CZTS /glass films among a outcome of annealed CZTS is provided in Fig. 4.

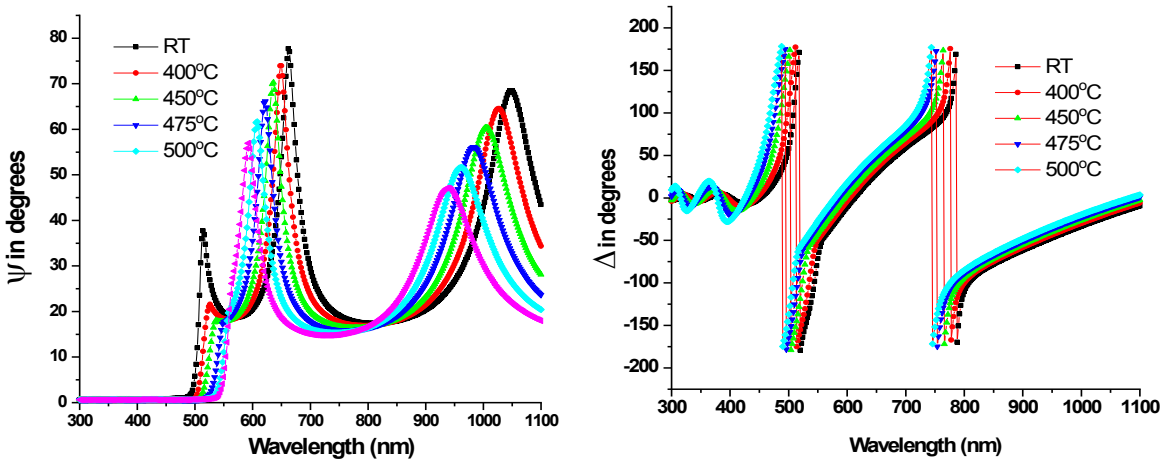

Fig. 4. Spectral ellipsometric data ψ & Δ for CZTS thin films at different annealing temperatures.

The optical values of n, k and d of the annealed CZTS films are determined by using least squares regression evaluation and mean square error function (MSE) to change the spectral dependence of ψ_{exp} & Δ_{exp} into the correct version to obtain unidentified fitting parameters and They rely most on borders. The Levenberg-Marquardt regression rule set is completely based on the record matching estimation and the modeling facts of ψ and Δ, and is used to reduce MSE and select the effectiveness of subsequent versions [32, 33]

$$MSE = \frac{1}{2\text{N-M}} \sum_{i=1}^{N} \left(\left(\frac{\psi_i^{\text{mod}} - \psi_i^{\text{exp}}}{\sigma_{\psi,i}^{\text{exp}}} \right)^2 + \left(\frac{\Delta_i^{\text{mod}} - \Delta_i^{\text{exp}}}{\sigma_{\Delta,i}^{\text{exp}}} \right)^2 \right) \tag{2}$$

In which, M is the appropriate parameters range and N is the number of ψ_{exp} & Δ_{exp} pairs included in the fitting, and that i is the index of summation. The The ψ_i^{exp}, Δ_i^{exp} and ψ_i^{mod}, Δ_i^{mod} are called the measured and modeled values, respectively. $\sigma_{\psi,i}^{\text{exp}}$ and $\sigma_{\Delta,i}^{\text{exp}}$ are the standard deviations of ψ_i^{exp}, Δ_i^{exp}, respectively.

The evaluation of SE records thru non-linear regression evaluation the use of a appropriate optical using Complete Ease SE software program [34]. In the existing examine, the model is built to provide a stacked-layer shape, that's particularly composed of 3 layers: a pitcher substrate, CZTS absorber layer, and a rough layer. The rough layer is modeled by using the effective medium approximation (EMA) that is the suitable device to establish the the morphology of the multilayer film configuration. More details about EMA are available and described in index [35]. Besides, the glass layer is modeled by using Cauchy version belt in Complete EASE software, while the CZTS layer is modeled with the aid of the usage of the B-spline computational process [36]. Fig. 5 (a, b) shows the spectral changes of $\psi_{exp.}$, Δ_{exp} of annealed CZTS /glass at RT and 500 ^{o}C, which are suited to the calculated ψ_i^{cal} and Δ_i^{cal} data received using the above recommended model. As the annealed temperature of the CZTS layer increased from RT to 500 ^{o}C, the fitting process produced a very low MSE value are 2.22 to 2.11, and the surface roughness of the CZTS film decreased from 5.22 nm to 3.82 nm. In addition, the interference pattern in the spectrum is caused by the coherence of a pair of reflections in the film [37]. The fitted optical constants, namely the refractive index, *n* and extinction coefficient, *k* of annealed CZTS films are shown in Figures 6 and 7 respectively.

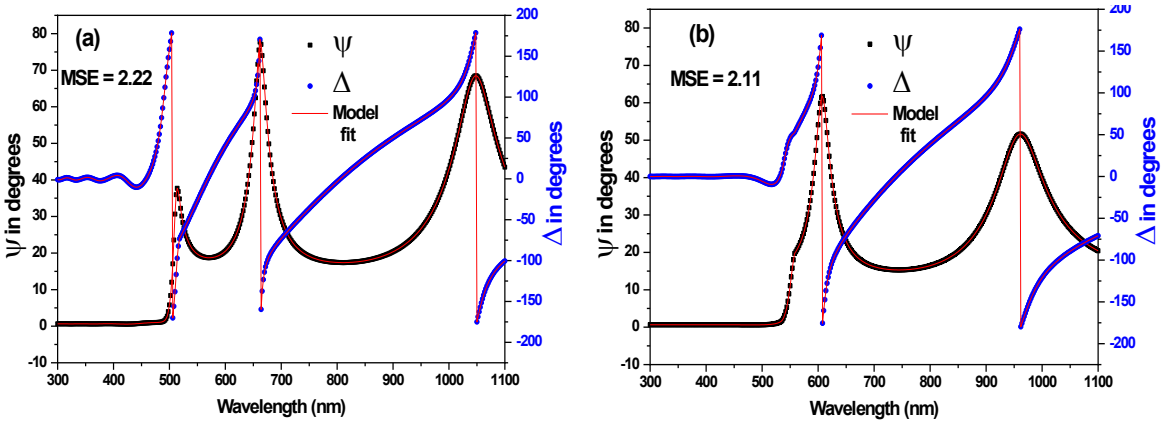

Fig. 5. Spectral ellipsometric data ψ and Δ for for CZTS thin films for (a) T = RT and (b) T= 500 ^{o}C grown on glass substrate. Experimental results are indicated by symbols, and the solid lines represent the model fit data.

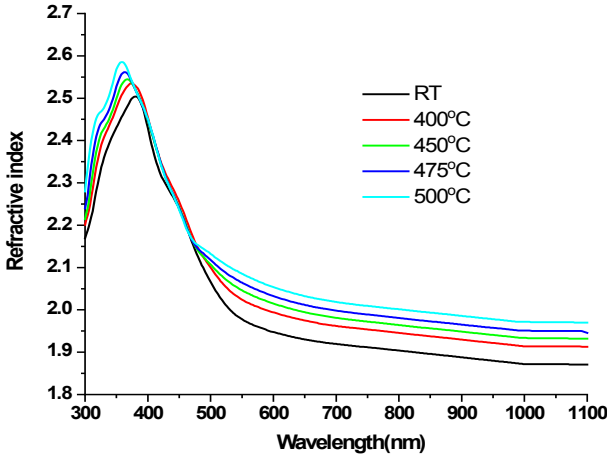

Fig. 6. Dispersion refractive index for CZTS thin films at different annealing temperatures.

In addition, it was observed that the refractive index increased with the increase of the annealing of the CZTS layer, which was attributed to the enhance in crystallinity, which led to the enhance in grain size [38].

Fig. 7 shows the k spectral behavior of CZTS/glass films with various annealing temperature obtained from the above model. Obviously, a significantly lower extinction coefficient is observed at the absorption edge, which confirms that the light is absolutely stopped in this variety [39].

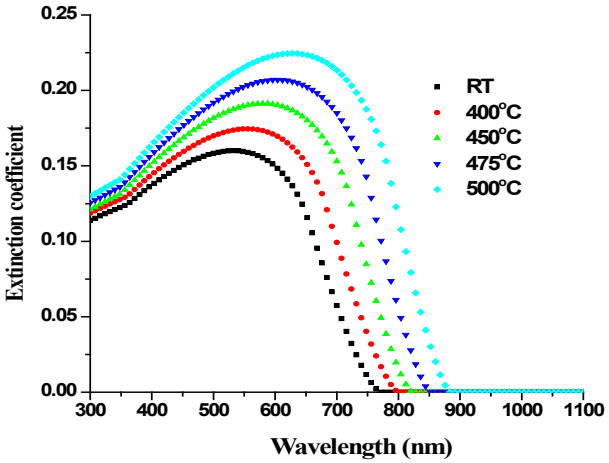

Fig. 7. Extinction coefficient versus wavelength for for CZTS thin films at different annealing temperatures.

The absorption coefficient *(α)* of different annealing temperature of CZTS /glass films was calculated in terms of k value that extracted from SE model via the subsequent relation $\alpha = 4\pi k/\lambda$ [40].

At strong absorption region, the optical energy band gap E_g^{opt} of varies annealing temperature of CZTS can be calculated using the Tauc relation of the following expression can be used [41]

$$(\alpha h\nu) = \alpha_o (h\nu - E_g)^p \quad (1)$$

where α_o and p are constant and exponent. Eq. 4 is the one that determines the type of optical transformations, whether they are allowed or not, depending on the value of the p-value; Since the CZTS film is polycrystalline, as shown by X-ray diffraction, the transition will most likely be permissible i.e. a p value of half (p = 1/2) [42-47]. Fig. 8 shows the relationship of $(\alpha h\nu)^2$ on the vertical axis with $h\nu$ on the horizontal axis of of different annealing of CZTS layer. The value of the gap energy, E_g^{opt} is determined by extending the line part of $(\alpha h\nu)^2$ to cut the horizontal axis, $h\nu$ at a zero value of $(\alpha h\nu)^2$, which is the value of the gap energy. Fig. 9 shows the energy gap values as a function of annealing temperature of CZTS film thickness It is observed that the value E_g^{opt} of CZTS/glass film decreases as the annealing temperature increases. Various informations have been published to explain that the band gap decreases with the increase of semiconductor annealing temperature, such as the quantum size effect [48,,49], structural parameters [50], the appearance of impurities [51, 52] and the reduction of stress and potential. In this study, the observed decrease of E_g^{opt} for CZTS/glass films with increasing annealing temperature is attributed to the enlarge in crysallize size, and fine lattice compaction.

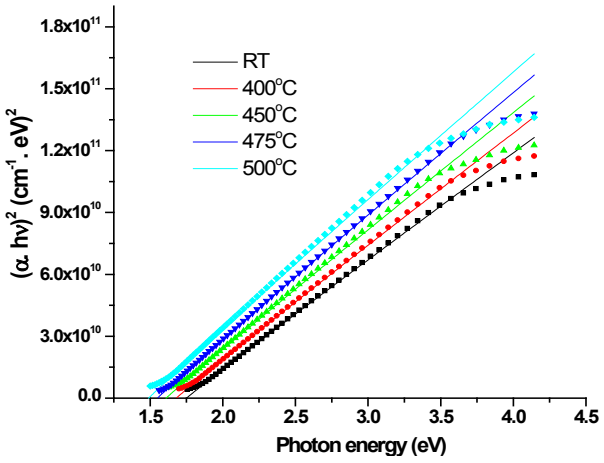

Fig. 8. Variations of $(\alpha h\nu)^2$ versus photon energy $(h\nu)$ for annealed CZTS thin films.

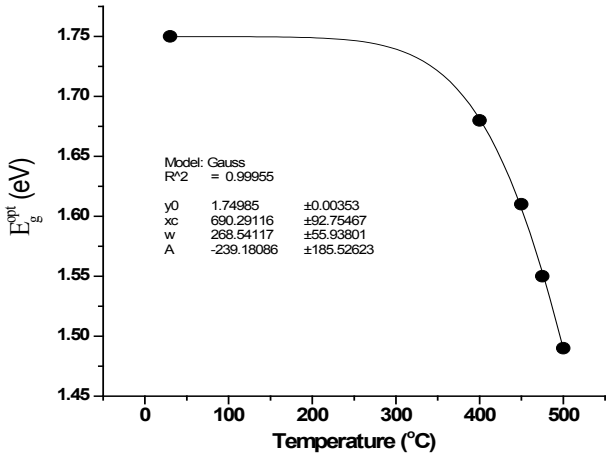

Fig. 9. Energy gap as a function of annealing temperature of CZTS thin films.

3.2. Dark and illuminated (I-V) characteristics of p-n junction

Fig. 10 illustrates the diagram of the studied p-n junction. It should be noted that the main parameters of the fabricated solar cells are extracted in the temperature range of RT–500 °C for CZTS to determine the behavior of dark (I-V) characteristics for the forward and reverse bias applied in the range of (−2 to 2 volts).

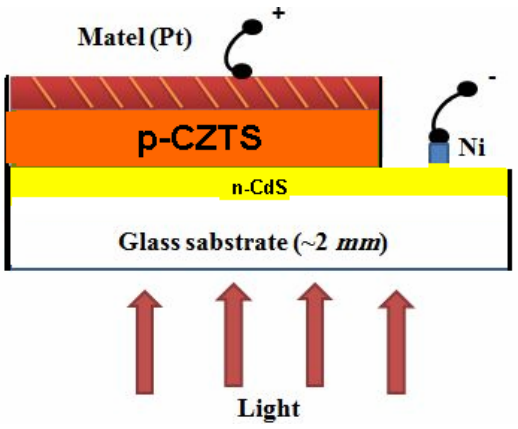

Fig. 10. The diagram of studied p-n junction n-CdS/p-CZTS Cell.

The current is related to the applied voltage.and the rest of the parameters of the fabricated diode are given by the following equation [53]:

$$I = I_{01}\left(\exp(\frac{q(V - IR_s)}{n_1 k_B T}) - 1\right) + I_{02}\left(\exp(\frac{q(V - IR_s)}{n_2 k_B T}) - 1\right) + \left(\frac{V - IR_s}{R_{sh}}\right) \quad (4)$$

In this formula: I_0 symbolizes the saturation current, n epitomizes the quality factor of the fabricated diode), q is the electronic charge which equals to $(1.6\times10^{-19}\ C)$ and k_B recaps the Boltzmann's constant. The rest parameters in Eq. (4) represent the parasitic resistances which includes the shunt resistance R_{sh} and series resistance R_s .

Fig. 11 depicts the dark (I-V) characteristics for the fabricated junction in forward and reverse bias for the variable annealing temperature p-CZTS into the n-CdS and applied voltage in the specified ranges. It is seen that the current increases as the annealing temperature increase to 500 °C. Fig. 12 depicts the dependence of the current on the applied voltage in the forward and reverse biases under AM 1.5 G illumination to highlight the high efficiency of the solar cell under investigation. The current in the forward bias voltage is higher than the current in the reverse bias voltage (I-V). These figures depict the increase in the current behavior of the solar cell generated in the case of the forward bias, which increases significantly in the low voltge region. It should be observed in the depletion region, that is, in the low voltage region, the exponential behavior of the reverse current of the examined manufactured solar cell is lower than the exponential behavior of the forward current in the same region. As a result, it can be reported that the fabricated solar cell has exceptional rectification characteristics.

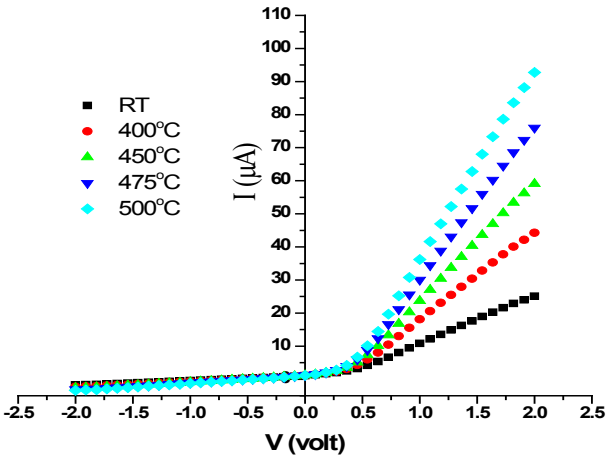

Fig. 11. The dark (I-V) charactristics for the fabricated solar cell.

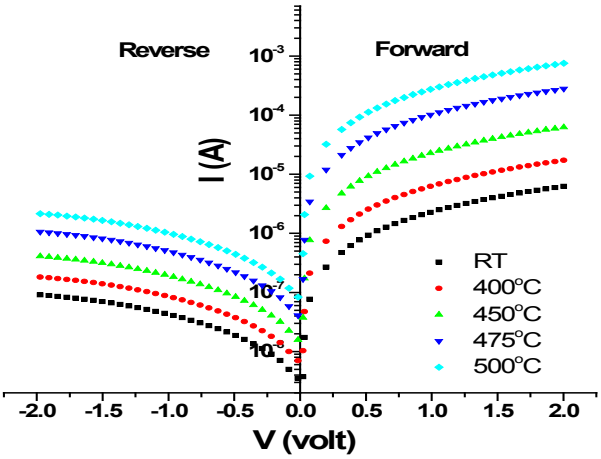

Fig. 12. Current versus the applied voltage for the p-n junction of solar cell at various annealing of CZTS in the range of (-2, 2) volts.

4. Conclusions

In this study, (CZTS) thin films have been prepared using the thermal evaporation technique. The effect of temperature on the structural, morphological and optical properties of CZTS thin films was investigated. XRD analysis reveals the Kesterite structure for the thin films. The crystallite size for CZTS thin films was in the range of (11-21 *nm*). The consequences received from SE display that the general behavior of the optical constants, *n* and *k* for the CZTS/glass film increases with the raise the annealing temperature. The outcomes in addition display that the E_g^{opt} with direct transition reduces (from 1.73 to 1,51 eV) as annealing temperature from RT nm to 500 ^{o}C.

It is accomplished that the optical constants of CZTS films enhance, as the annealing temperature of CZTS increments. The Ni/n-CdSe/p-CdTe/Pt heterojunction has been assembled. The dark and illumination (current-voltage) traits of fabricated heterojunctions had been suggested at distinctive different annealing of CZTS layer, as well as for voltages ranging from -2 to 2 volts. The increase in the current behavior of the p-n junction generated in the case of the forward bias, which increases significantly in the low voltge region. It should be observed in the depletion region, that is, in the low voltage region, the exponential behavior of the reverse current of the examined manufactured solar cell is lower than the exponential behavior of the forward current in the same region. As a result, it can be reported that the fabricated solar cell has exceptional rectification characteristics.

Acknowledgments

The researchers wish to extend their sincere gratitude to the Deanship of Scientific Research at the Islamic University of Madinah for the support provided to the Post-Publishing Program 1.

References

[1] Husain, A. A., Hasan, W. Z. W., Shafie, S., Hamidon, M. N., & Pandey, S. S. (2018). A review of transparent solar photovoltaic technologies. Renewable and sustainable energy reviews, 94, 779-791.; https://doi.org/10.1016/j.rser.2018.06.031

[2] Liu, J., Zhang, M., & Feng, X. (2018). Simulation of graded bandgap on the performance of

back-wall superstrate CIGS solar cells. Optik, 172, 1172-1178; https://doi.org/10.1016/j.ijleo.2018.07.084

[3] Ren, S., Wang, H., Li, Y., Li, H., He, R., Wu, L. & Feng, L. (2018). Rapid thermal annealing on ZnMgO window layer for improved performance of CdTe solar cells. Solar Energy Materials and Solar Cells, 187, 97-103; https://doi.org/10.1016/j.solmat.2018.06.033

[4] Chen, S., Gong, X. G., Walsh, A., & Wei, S. H. (2009). Crystal and electronic band structure of Cu 2 ZnSn X 4 (X= S and Se) photovoltaic absorbers: First-principles insights. Applied Physics Letters, 94(4), 041903; https://doi.org/10.1063/1.3074499

[5] Agawane, G. L., Kamble, A. S., Vanalakar, S. A., Shin, S. W., Gang, M. G., Yun, J. H., & Kim, J. H. (2015). Fabrication of 3.01% power conversion efficient high-quality CZTS thin film solar cells by a green and simple sol-gel technique. Materials Letters, 158, 58-61; https://doi.org/10.1016/j.matlet.2015.05.036

[6] Fernandes, P. A., Salomé, P. M. P., & Da Cunha, A. F. (2010). CuxSnSx+ 1 (x= 2, 3) thin films grown by sulfurization of metallic precursors deposited by dc magnetron sputtering. physica status solidi c, 7(3-4), 901-904; https://doi.org/10.1002/pssc.200982746

[7] Salomé, P. M. P., Malaquias, J., Fernandes, P. A., Ferreira, M. S., Da Cunha, A. F., Leitão, J. P., & Matinaga, F. M. (2012). Growth and characterization of Cu2ZnSn (S, Se) 4 thin films for solar cells. Solar Energy Materials and Solar Cells, 101, 147-153; https://doi.org/10.1016/j.solmat.2012.02.031

[8] Swami, S. K., Kumar, A., & Dutta, V. (2013). Deposition of kesterite Cu2ZnSnS4 (CZTS) thin films by spin coating technique for solar cell application. Energy Procedia, 33, 198-202; https://doi.org/10.1016/j.egypro.2013.05.058

[9] Seol, J. S., Lee, S. Y., Lee, J. C., Nam, H. D., & Kim, K. H. (2003). Electrical and optical properties of Cu2ZnSnS4 thin films prepared by rf magnetron sputtering process. Solar Energy Materials and Solar Cells, 75(1-2), 155-162; https://doi.org/10.1016/S0927-0248(02)00127-7

[10] Jimbo, K., Kimura, R., Kamimura, T., Yamada, S., Maw, W. S., Araki, H., ... & Katagiri, H. (2007). Cu2ZnSnS4-type thin film solar cells using abundant materials. Thin solid films, 515(15), 5997-5999; https://doi.org/10.1016/j.tsf.2006.12.103

[11] Liu, F., Li, Y., Zhang, K., Wang, B., Yan, C., Lai, Y., & Liu, Y. (2010). In situ growth of Cu2ZnSnS4 thin films by reactive magnetron co-sputtering. Solar Energy Materials and Solar Cells, 94(12), 2431-2434; https://doi.org/10.1016/j.solmat.2010.08.003

[12] Weber, A., Krauth, H., Perlt, S., Schubert, B., Kötschau, I., Schorr, S., & Schock, H. W. (2009). Multi-stage evaporation of Cu2ZnSnS4 thin films. Thin Solid Films, 517(7), 2524-2526; https://doi.org/10.1016/j.tsf.2008.11.033

[13] Gunawan, O., Todorov, T. K., & Mitzi, D. B. (2010). Loss mechanisms in hydrazine-processed Cu 2 ZnSn (Se, S) 4 solar cells. Applied Physics Letters, 97(23), 233506; https://doi.org/10.1063/1.3522884

[14] Moriya, K., Tanaka, K., & Uchiki, H. (2008). Cu2ZnSnS4 thin films annealed in H2S atmosphere for solar cell absorber prepared by pulsed laser deposition. Japanese Journal of Applied Physics, 47(1S), 602; https://doi.org/10.1143/JJAP.47.602

[15] Pawar, S. M., Moholkar, A. V., Kim, I. K., & Shin, S. W. (2010). JH moon, JI Rhee and JH Kim: Curr. Appl. Phys, 10, 565-569; https://doi.org/10.1016/j.cap.2009.07.023

[16] Katagiri, H., Saitoh, K., Washio, T., Shinohara, H., Kurumadani, T., & Miyajima, S. (2001). Development of thin film solar cell based on Cu2ZnSnS4 thin films. Solar Energy Materials and Solar Cells, 65(1-4), 141-148; https://doi.org/10.1016/S0927-0248(00)00088-X

[17] Daranfed, W., Aida, M. S., Attaf, N., Bougdira, J., & Rinnert, H. (2012). Cu2ZnSnS4 thin films deposition by ultrasonic spray pyrolysis. Journal of alloys and compounds, 542, 22-27; https://doi.org/10.1016/j.jallcom.2012.07.063

[18] Valdes, M., Santoro, G., & Vázquez, M. (2014). Spray deposition of Cu2ZnSnS4 thin films. Journal of Alloys and Compounds, 585, 776-782; https://doi.org/10.1016/j.jallcom.2013.10.009

[19] Shinde, N. M., Deokate, R. J., & Lokhande, C. D. (2013). Properties of spray deposited

Cu2ZnSnS4 (CZTS) thin films. Journal of Analytical and Applied Pyrolysis, 100, 12-16; https://doi.org/10.1016/j.jaap.2012.10.018

[20] K. Sun, C. Yan, F. Liu, et al. Over 9% Efficient Kesterite Cu2ZnSnS4 Solar Cell Fabricated by Using Zn1-xCdxS Buffer Layer[J]. Advanced Energy Materials, 2016, 6, 1600046; https://doi.org/10.1002/aenm.201600046

[21] Y. S. Lee, T. Gershon, O. Gunawan, et al. Cu2ZnSnSe4 Thin-Film Solar Cells by Thermal Co-evaporation with 11.6% Efficiency and Improved Minority Carrier Diffusion Length[J]. Advanced Energy Materials, 2015, 5, (7); https://doi.org/10.1002/aenm.201401372

[22] W. Wang, M. T. Winkler, O. Gunawan, et al. Device Characteristics of CZTSSe Thin-Film Solar Cells with 12.6% Efficiency[J]. Advanced Energy Materials, 2014, 4, 1301465; https://doi.org/10.1002/aenm.201301465

[23] M. A. Green, K. Emery, Y. Hishikawa, et al. Solar cell efficiency tables (Version 46)[J]. Progress in photovoltaics: research and applications, 2015, 23: 805-812; https://doi.org/10.1002/pip.2637

[24] Weber, A., Mainz, R., & Schock, H. W. (2010). On the Sn loss from thin films of the material system Cu-Zn-Sn-S in high vacuum. Journal of Applied Physics, 107(1), 013516; https://doi.org/10.1063/1.3273495

[25] A. Almohammedi, A. Ashour, E. R. Shaaban, Structural, morphological and optical properties of annealed Cu2ZnSnS4 thin films using the first derivative of TGA curve for solar cell applications, Journal of Ovonic Research, 16(1), (2020) 21-27

[26] Barkhouse, D. A. R., Gunawan, O., Gokmen, T., Todorov, T. K., & Mitzi, D. B. (2012). Device characteristics of a 10.1% hydrazine-processed Cu2ZnSn (Se, S) 4 solar cell. Progress in Photovoltaics: Research and Applications, 20(1), 6-11; https://doi.org/10.1002/pip.1160

[27] Todorov, T. K., Tang, J., Bag, S., Gunawan, O., Gokmen, T., Zhu, Y., & Mitzi, D. B. (2013). Beyond 11% efficiency: characteristics of state-of-the-art Cu2ZnSn (S, Se) 4 solar cells. Advanced Energy Materials, 3(1), 34-38; https://doi.org/10.1002/aenm.201200348

[28] Sun, L., He, J., Chen, Y., Yue, F., Yang, P., & Chu, J. (2012). Comparative study on Cu2ZnSnS4 thin films deposited by sputtering and pulsed laser deposition from a single quaternary sulfide target. Journal of Crystal Growth, 361, 147-151; https://doi.org/10.1016/j.jcrysgro.2012.09.023

[29] H.G. Tompkins, J.N. Hilfiker, Spectroscopic Ellipsometry Practical Application to Thin Film Characterization, Momentum press LLC, New York, 2016.

[30] H. Fujiwara, Spectroscopic Ellipsometry Principles and Applications, John Wiley & Sons Ltd, West Sussex, England, 2007.

[31] G. E. Jellison,Spectroscopic ellipsometry data analysis, measured versus calculated quantities,Thin Solid Films. 313-314 (1998) P.P 33-39; https://doi.org/10.1016/S0040-6090(97)00765-7

[32] Guide to use CompleteEase software manual version (6.51): Data acquisition and analysis software for J. A. Woollam spectroscopic ellipsometers, 2017.

[33] M. Zhao, R. Tong, X. Chen, T. Ma, J. Dai, J. Lian, J. Ye, Ellipsometric determination of anisotropic optical constants of single phase Ga2O3 thin films in its orthorhombic and monoclinic phases, Opt. Mater.102 (2020) P.109807-109814; https://doi.org/10.1016/j.optmat.2020.109807

[34] D. Amans, S. Callard, A. Ganarie, and J. Joseph,Ellipsometric study of silicon nanocrystal optical constants, J. Appl. Phys. 93, (2003) P.P 4173-4179; https://doi.org/10.1063/1.1538344

[35] B. Gallas, C.-C. Kao, C. Defranoux, S. Fisson, G. Vuye, and J. Rivory, Dielectric function of Si nanocrystals embedded in SiO2, Thin Solid Films 455-456, 335 (2004). P.P 335-338; https://doi.org/10.1016/j.tsf.2003.11.198

[36] L. Ding, T. P. Chen, Y. Liu, C. Y. Ng, and S. Fung,Optical properties of silicon nanocrystals embedded in a SiO2 matrix, Physical Review B 72 (2005) P.P 125409-125414; https://doi.org/10.1103/PhysRevB.72.125419

[37] Behzadi, F., Saievar-Iranizad, E., & Pakizeh, E. (2018). Optical study on single-layer photoluminescent graphene oxide nanosheets through a simple and green hydrothermal method. Journal of Photochemistry and Photobiology A: Chemistry, 364, 595-601; https://doi.org/10.1016/j.jphotochem.2018.06.047

[38] Pakizeh, E., & Moradi, M. (2018). Effect of particle size on the optical properties of lead zirconate titanate nanopowders. Journal of the American Ceramic Society, 101(12), 5335-5345; https://doi.org/10.1111/jace.15792

[39] E. R. Shaaban, M. S. Abd El-Sadek, M. El-Hagary, I. S. Yahia, Spectroscopic ellipsometry investigations of the optical constants ofnanocrystalline SnS thin films, Physica Scripta 86 (1) (2012) 015702; https://doi.org/10.1088/0031-8949/86/01/015702

[40] ER Shaaban, YAM Ismail, HS Hassan, Compositional dependence of the optical properties of amorphous SeTe Bi thin films using transmittance and reflectance Journal of non-crystalline solids 376, 61 (2013); https://doi.org/10.1016/j.jnoncrysol.2013.05.024

[41] Prakash, D., Aboraia, A.M., El-Hagary, M., Shaaban, E.R., Verma, K.D., Determination of the optical constants and film thickness of ZnTe and ZnS thin films in terms of spectrophotometric and spectroscopic ellipsometry, Ceramics International 42(2) (2016) 2676; https://doi.org/10.1016/j.ceramint.2015.10.096

[42] ElS Yousef, A. El-Adawy, N. El Koshkhany, E. R.Shaaban, Optical and acoustic properties of TeO2 /WO3 glasses with small amount of additive ZrO2, Journal of Physics and Chemistry of Solids., 67(2006)1649-1655; https://doi.org/10.1016/j.jpcs.2006.02.014

[43] El-Kabnay, N., Shaaban, E.R., Afify, N., Abou-sehly, A.M. Optical and physical properties of different composition of Inx Se1-x thin films, Physica B: Condensed Matter, 403 (1) (2008) 31-36; https://doi.org/10.1016/j.physb.2007.08.016

[44] Qasem, A., Hassan, A. A., Rajhi, F. Y., Abbas, H. A. S., & Shaaban, E. R. (2022). Effective role of cadmium doping in controlling the linear and non-linear optical properties of non-crystalline Cd-Se-S thin films. Journal of Materials Science: Materials in Electronics, 33(4), 1953-1965; https://doi.org/10.1007/s10854-021-07400-5

[45] Khare, A., Wills, A. W., Ammerman, L. M., Norris, D. J., & Aydil, E. S. (2011). Size control and quantum confinement in Cu 2 ZnSnS 4 nanocrystals. Chemical communications, 47(42), 11721-11723; https://doi.org/10.1039/c1cc14687d

[46] Qasem, A., Alshahrani, B., Yakout, H. A., Abbas, H. A. S., & Shaaban, E. R. (2021). Tuning structural, optical, electrical and photovoltaic characteristics of n-type CdS1− xSbx layers for optimizing the performance of n-(CdS: Sb)/p-Si solar cells. Applied Physics A, 127(11), 1-13; https://doi.org/10.1007/s00339-021-04999-4

[47] Alshahrani, B., Nabil, S., Elsaeedy, H. I., Yakout, H. A., & Qasem, A. (2021). The Pivotal Role of Thermal Annealing of Cadmium Telluride Thin Film in Optimizing the Performance of CdTe/Si Solar Cells. Journal of Electronic Materials, 50(8), 4586-4598; https://doi.org/10.1007/s11664-021-08989-3

[48] Elsaeedy, H. I., Qasem, A., Yakout, H. A., & Mahmoud, M. (2021). The pivotal role of TiO2 layer thickness in optimizing the performance of TiO2/P-Si solar cell. Journal of Alloys and Compounds, 867, 159150; https://doi.org/10.1016/j.jallcom.2021.159150

[49] Jhaveri, Janam, Interface Recombination in TiO2/Silicon Heterojunctions for Silicon Photovoltaic Applications, Diss. Princeton University, 2018.

[50] Li, C., Song, Z., Zhao, D., Xiao, C., Subedi, B., Shrestha, N., ... & Yan, Y. "Reducing saturation-current density to realize high-efficiency low-bandgap mixed tin-lead halide perovskite solar cells." Advanced Energy Materials 9.3 (2019): 1803135; https://doi.org/10.1002/aenm.201803135

[51] Gacio, D., Alonso, J. M., Garcia, J., Perdigao, M. S., Saraiva, E. S., & Bisogno, F. E, Effects of the junction temperature on the dynamic resistance of white LEDs, IEEE Trans. Ind. Appl. 49 (2) (2013) 750-760; https://doi.org/10.1109/TIA.2013.2243092

[52] Qasem, A., Alrafai, H. A., Alshahrani, B., Said, N. M., Hassan, A. A., Yakout, H. A., &

Shaaban, E. R. (2022). Adapting the structural, optical and thermoelectrical properties of thermally annealed silver selenide (AgSe) thin films for improving the photovoltaic characteristics of the fabricated n-AgSe/p-CdTe solar cells. Journal of Alloys and Compounds, 899, 163374; https://doi.org/10.1016/j.jallcom.2021.163374

[53] Qasem, A., Mahmoud, M., Elsaeedy, H. I., Mostafa, M. S., & Shaaban, E. R. (2021). Effective role of temperature in improving the structural, optical and photovoltaic characteristics for n-Zn0. 5Cd0. 5Te/p-CdTe solar cells. Optical Materials, 111746; https://doi.org/10.1016/j.optmat.2021.111746